UNCLASSIFIED

AD 220 210

UNCLASSIFIED

123599

FUNDAMENTALS OF ULTRASONIC WELDING

PHASE II

Bimonthly Progress Report No. 1

February 15, 1959

Prepared under Navy, Bureau of Aeronautics
Contract NOas 59-6070-c

AEROPROJECTS INCORPORATED
WEST CHESTER, PENNSYLVANIA

FC
BAC

ASTIA

FUNDAMENTALS OF ULTRASONIC WELDING

PHASE II

February 15, 1959

Prepared under Navy, Bureau of Aeronautics
Contract NOas 59-6070-c

Bimonthly Progress Report No. 1

December 16, 1958, to February 15, 1959

The Information Contained in This
Progress Report is Preliminary and
Subject to Revision or Modification.

AEROPROJECTS INCORPORATED
West Chester, Pennsylvania

DISTRIBUTION LIST

No. of Copies

50
+ Reproducible
Department of the Navy
Bureau of Aeronautics
Airborne Equipment Division
Washington 25, D.C.
Attn: AE-416

12
Department of Navy
Bureau of Aeronautics
Technical Data Division
Washington 25, D. C.
Attn: TD-4106

1
Bureau of Aeronautics Representative
100 Woodland Avenue
Morton, Pennsylvania

ABSTRACT

Phase I of the program wherein photoelastic, ultrasonic power measurement, and temperature determining methods were developed to implement study of the ultrasonic welding mechanism, is reviewed. The current effort involves analysis of the transient internal stress pattern associated with formation of such bonds, the arrangement of various metals and alloys into an "order of weldability" based on power required to make a weld and consideration of the various metallurgical phenomena that have been observed in vibratory welds.

i

TABLE OF CONTENTS

LIST OF FIGURES

LIST OF FIGURES (Concluded)

LIST OF TABLES

I. INTRODUCTION

The object of this research program is to develop a phenomenological theory of ultrasonic welding that will account for the observed effects and that can be used to improve the design of ultrasonic welding equipment and extend its usefulness in joining the newer, high-temperature, corrosion-resistant materials of particular significance to the various military and Atomic Energy programs.

Phase I of this investigation involved the development of special in-strumentation and techniques implicit in excavating and interpreting in-formation from observable interacting factors involved in the ultrasonic welding process. It included preliminary study of certain ultrasonic weld phenomena and considered the influence of material properties on welda-bility. In particular,

(a) Accumulated evidence having shown that ultrasonic welding may be accomplished at least in part, as a result of deformation at and near the interface being joined, it was clear that understanding of the transient stresses producing such deformation is important. Thus, photoelastic techniques were considered and later developed, so that the internal dynamic stress pattern associated with the applied static and superimposed oscillating shear force associated with welding could be observed and photographed. A special strain frame for applying the requisite force system was devised and routinely utilized. Recourse to the laborious frozen stress tech-nique was obviated by development of direct observation triaxially restrained photoelastic models. This work was carried far enough that its usefulness in studying this facet of the welding process was reasonably well established.

(b) It being self evident that a theory of the mechanism of vibratory welding must consider the energy required to produce a weld, the Phase I work considered avenues by which we could ascertain net power and the instantaneous values thereof in time, during which a weld was generated. No practical method for measuring trans-mitted ultrasonic power was available but analysis indicated a standing elastic wave measurement technique to be possible and capable of standard oscillographic data recording. The method was developed, its validity established in calorimetric experi-ments, and its use reduced to routine. It is to be noted that this approach is inclusive; e.g., knowing frequency, power and its variation in time, such ancillary variables as tip amplitude are easily obtained when there is reason to know it. More im-portant, the actual weld impedance during formation can be ascer-tained and this is fundametal to developing the process and equipment to implement it. Consideration was given to determining the energy passing through and beyond the weld zone, since this too is included but must be deducted, from the transmitted ultrasonic power data obtained with the SWR technique.

1

(c) It being well known that there is a temperature rise of some magnitude during the formation of an ultrasonic weld, the need for reliable information on weld zone heating and necessity for correlation thereof with the process variables was obvious. Material properties are transiently affected by heat; recrystallization, diffusion, phase change and the possible interaction of such normal metallurgical phenomena with vibratory stresses, all pointed to the need for a practical technique to determine transient temperatures at the weld zone interface. Accordingly, a single fine wire thermocouple technique was developed to accomplish sensing, from which rapid response equipment produced reproducible records. The technique was utilized to obtain preliminary but significant information on the process variables — power, clamping force, and weld time for the materials, copper, aluminum and iron. Validity of the temperatures obtained was confirmed by means of a meltable insert technique.

(d) Explorations were made into the characteristic of the interface disturbance routinely observed in ultrasonic welds in various materials and several metallurgical phenomena including recrystallization and diffusion were noted. This facet of Phase I served to orient much of the work that will be carried out as Phase II progresses. An autoradiographic technique involving Beta emission was utilized experimentally as a candidate technique for studying interfacial displacements where standard metallography is inadequate. Lower energy Beta radiation was deemed essential to obtaining meaningful information in the course of this Phase II. Metal displacement, recrystallization, diffusion, phase transformation, and miscellaneous effects were noted in various materials.

(e) A statistical approach to define the relation of material properties to ultrasonic weldability was considered at length, but the complexity thereof and time involved appeared to be excessive. Success in developing the SWR method for measuring the net energy required to generate a weld suggested a less complex method; e.g., that an "order of weldability" in terms of energy and material thickness should yield a correlation with certain material properties which could be determined by systematic analysis of material properties data, including properties at temperature. It was determined that the net energy involved in generating a weld of a unit area between, for example, two sheets of 0.001-inch thickness aluminum, and stainless steel, embraced a large range — in the order of 1 to 100 watts, respectively, with copper sheets of the same thickness falling between.

On the basis of preliminary data acquired in Phase I, it is concluded this approach merits aggressive pursuit.

2

II. CURRENT EFFORT

A. STRESS DISTRIBUTION IN THE WELD ZONE

Phase I of this aspect of the investigation accomplished the development of a strain frame for loading photoelastic models in a fashion to essentially duplicate any instantaneous loading condition associated with the actual accomplishment of a bond between two pieces of sheet metal by means of ultrasonic welds (1)*.

Suitable direct observation triaxially restrained photoelastic models were developed which permit observation of a changing stress pattern (2). Motion pictures showing the changing stress pattern as it can be observed with such triaxially restrained models, were obtained. It was observed that when the "welding" tip reaches the stick-slip condition, very rapid and significant changes take place in the stress pattern. With these models, resort to the laborious frozen stress technique can, within practical limits, be obviated.

A simple plank model was shown to be sufficiently similar to the triaxially restrained model that it can be used with reasonable accuracy for study of static conditions associated with normal loading, normal plus transverse loading just prior to slip, and normal plus transverse loading just after slip. As the work progresses and the weld-producing stresses are understood, the triaxially restrained models will be utilized to modify the data obtained from the plank models by inspection.

Literature study disclosed information on point-loaded models only (3, 4, and 5) and nothing more parallel to the situation existent in ultrasonic weld geometry appears to have been published. Adequate understanding of the situation should include differentiating local slip from gross sliding, and requires detailed analysis of photographic data obtained from photoelastic models loaded as outlined above so as to provide evidence of both normal stress (σ_y) and shearing stress (τ_{xy}) distribution at the affected interface.

Such complete photoelastic analysis is not usually done, ordinarily being carried but far enough to obtain the maximum shearing stress gradient (by counting fringes). When the principal stresses must be evaluated, it is necessary to make a comprehensive analysis, as in this case.

Accordingly, the following investigation is in progress:

Photoelastic plank models similar to those described in Phase I, Progress Report No. 2, Figure 2, are being loaded under the following conditions:

* Numbers in parenthesis indicate items in the List of References at the end of the report.

3

a. Tip radius, 30-6 (equivalent to 3-inch tip radius on 0.050-inch metal sheet)

b. Normal force, 300 pounds

c. Lateral force at "stick-before-slip", 76-80 pounds

d. Lateral force just after slip, 85-90 pounds

Fringe patterns are photographed and isoclinic patterns are photographed at 15-degree increments in polarizing angle. From these data the normal and shearing stress values are obtained analytically by utilizing equations from Lee (6) as follows:

$$\tau_{xy} = 1/2\ (\sigma_1 - \sigma_2)\ \sin 2\ \phi \qquad (1)$$

$$\sigma_{x_1} - \sigma_{x_0} + \int_{x\ =\ 0}^{x\ =\ x_1} \frac{\partial \tau_{xy}}{\partial y}\ dx = 0 \qquad (2)$$

$$\sigma_y = \sigma_x \pm \sqrt{(\sigma_1 - \sigma_2)^2 - (4\tau_{xy})^2} \qquad (3)$$

where τ_{xy} is shearing stress,

$\sigma_1 - \sigma_2$ is difference in the principal stresses,

ϕ is angle of isoclinic,

σ_{x_1} is component of principal stresses along the x axis

σ_{x_0} is component of principal stresses at original selected σ_{x_1}

$\dfrac{\partial \tau_{xy}}{\partial y}$ is shearing stress gradient in y direction at point of interest.

σ_y is the normal stress.

The resulting information is being plotted, as in Figure 1 which qualitatively illustrates accumulating data for the single case of normal plus transverse loading just prior to slip. It presently appears, on the basis of incomplete plots, that the shear stress at the interface on one side of the axis is almost completely relieved during half of the excursion cycle; whereas, the shear stress at the interface on the opposite side of the axis is greatly increased. When the shearing stress locally exceeds the maximum possible "non-slip" shearing stress in some locale, local slip, but not gross sliding, will occur.

The trend of information from the photoelastic studies is throwing light on past observations that have not been completely understood, such as, for example, the unbonded central area found in welds between fairly thick sheets of material; the apparently differing performance of the reed-wedge coupling system over the lateral drive horn-type coupling system, which is soft in bending.

SYSTEM
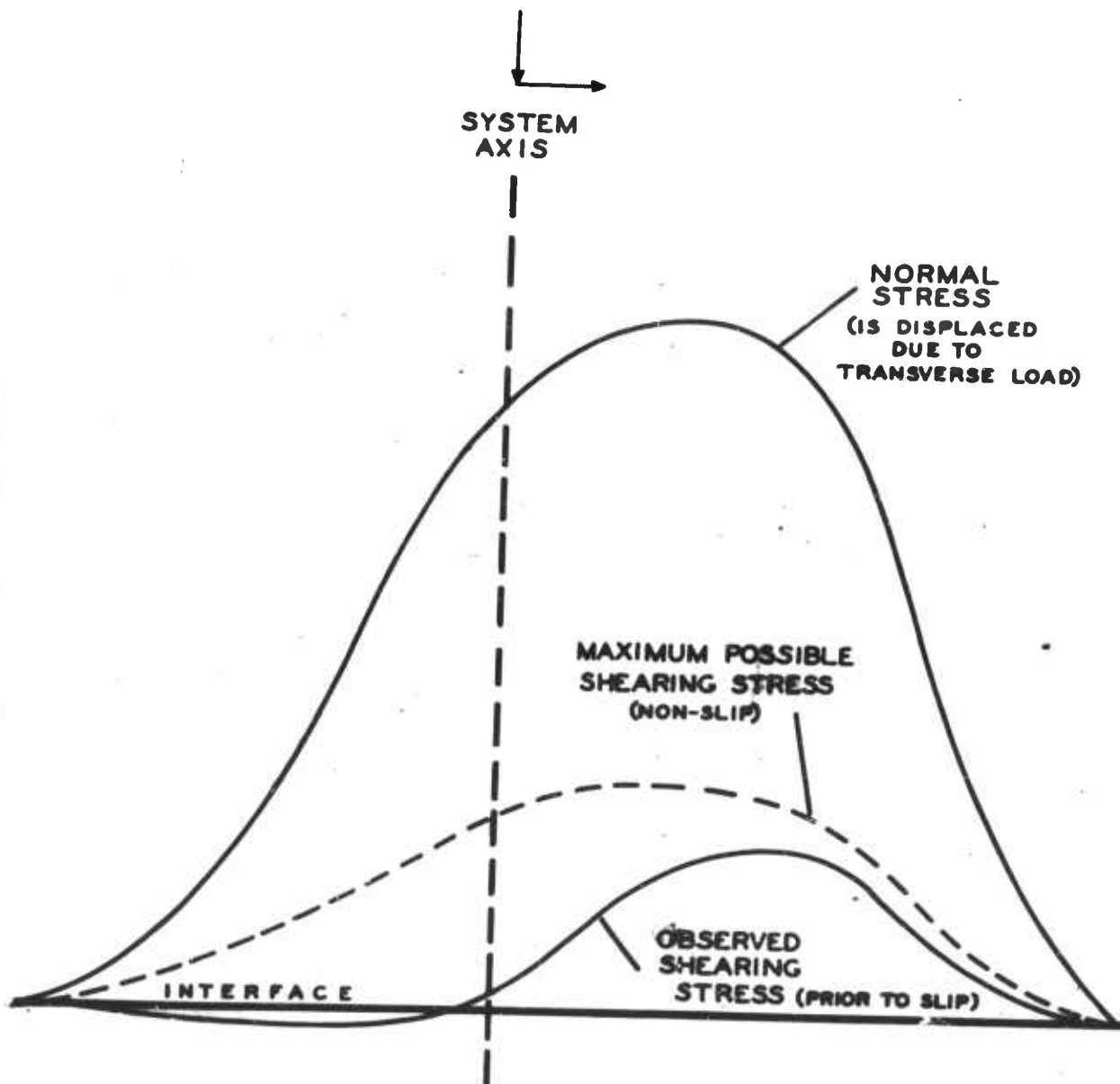AXIS

NORMAL
STRESS
(IS DISPLACED
DUE TO
TRANSVERSE LOAD)

MAXIMUM POSSIBLE
SHEARING STRESS
(NON-SLIP)

OBSERVED
SHEARING
STRESS (PRIOR TO SLIP)

INTERFACE

FIGURE 1. SEMI-HYPOTHETICAL STRESS DISTRIBUTION
FOR COMBINED NORMAL AND TRANSVERSE LOAD

5

B. MICROSTRUCTURE

As research into the fundamentals of ultrasonic welding proceeds into this advanced phase, it is desirable to review and recap certain microstructural characteristics that have been observed in various materials from time to time as this joining process has evolved.

Bonding can occur without sufficient local heat generation to be detectable in the microstructure. Bonds of this sort exhibit interpenetration of the mating surfaces and/or mechanical disruption of surface films. Examples are shown in Figures 2 and 3.

In Figure 2a, note the high degree of interpenetration. In one area, the Kovar has intruded approximately 75% of the nickel thickness. The gold-plated surface of the Kovar has been dispersed through the highly worked regions. There are no discontinuities along the interface despite the large interpenetration. The second phase in the Kovar tends to line up in "strings" in the worked regions and is unaffected in the remainder of the material.

In Figure 2b, the interfacial riplets of the nickel-molybdenum weld are a striking example of the plastic flow which occurs locally. Entrapped oxide can be seen by the dark patches on the right. It is extremely difficult and often impossible to differentiate between cold flow and recrystallisation by optical means in such localised regions. There is a vague periodicity in the ripples at the interface.

In Figure 3a, the interpenetration of the titanium-beryllium weld is another example of the mutual surface deformation which may often be observed in dissimilar metal welds. The swirls characteristic of Figures 2a and 2b can be observed to occur on a small scale along the interface.

Figure 3b illustrates the oxide dispersion which occurs during the bonding of 0.012-inch 1100-H14 aluminum sheets.

Dissimilar metal welds may also exhibit obvious microstructural changes resulting from heat generated in the material during the formation of the bond. A typical example is shown in Figure 4, in which the acicular structure of the titanium alloy resulted from exceeding the Beta-transformation temperature. The photograph was taken near the edge of the weld spot. Notice the curvature of the transformed zone as it approaches the edge of the spot. Observe the intermetallic compound formed along the interface and the diffusion gradient at the edge of the heat-affected zone.

Figures 5a and 5b are examples of localized recrystallisation. The surface film is periodically dispersed along the interface and recrystallisation and growth has occurred in these regions.
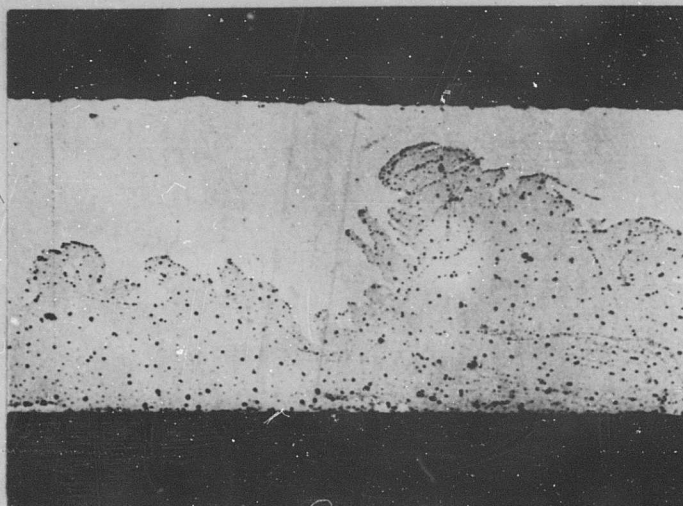
(a) Nickel and Gold-Plated Kovar
(0.003-in. thicknesses)

Unetched
Magnification: 300X
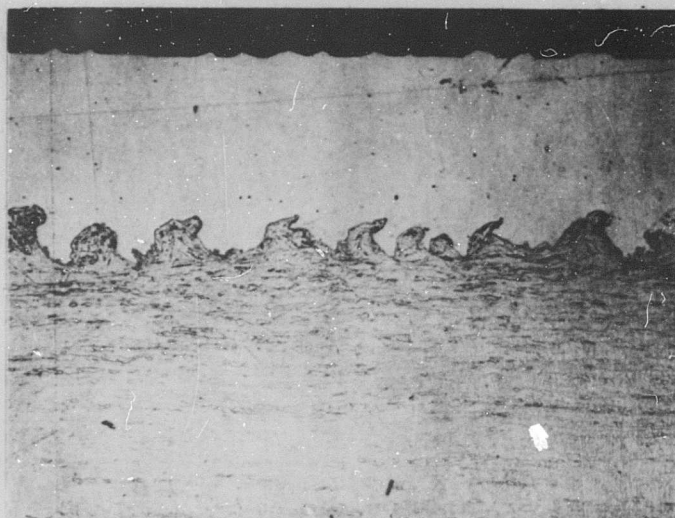
(b) Nickel (0.005 in. thick) and Molybdenum
(0.020 in. thick)--Showing Local Plastic Flow

Etchant: KOH + $K_3(CN)_6$
Magnification: 300X

Figure 2. PHOTOMICROGRAPHS OF INTERPENETRATION OF MATING SURFACES
OF DISSIMILAR METALS AFTER ULTRASONIC WELDING -

(a) Titanium (0.003 in. thick) and
Beryllium (0.050 in. thick)

Etchant: HNO_3 + HF + H_2O
Magnification: 400X
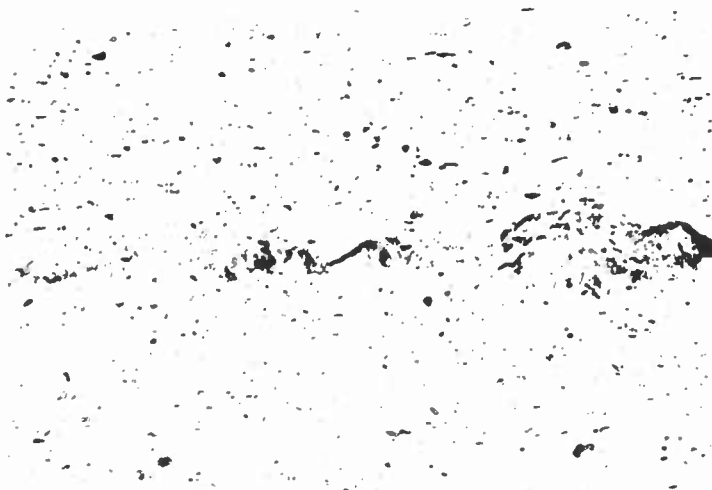
(b) 1100-H14 Aluminum Sheets (0.012 in. thick)--
Showing Mechanical Dispersion of Surface Film

Etchant: 0.5% HF
Magnification: 500X

Figure 3. PHOTOMICROGRAPHS OF INTERPENETRATION OF MATING SURFACES
OF DISSIMILAR METALS AFTER ULTRASONIC WELDING

Figure 4. PHOTOMICROGRAPH OF INTERPENETRATION OF MATING SURFACES
OF 430 STAINLESS STEEL (0.024 in. thick) AND A-110-AT
TITANIUM ALLOY (0.028 in. thick)--SHOWING STRUCTURAL
CHANGES IN THE TITANIUM ALLOY RESULTING FROM HEAT GEN-
ERATED DURING ULTRASONIC WELDING

Etchant: HF + HNO$_3$
Magnification: 150X
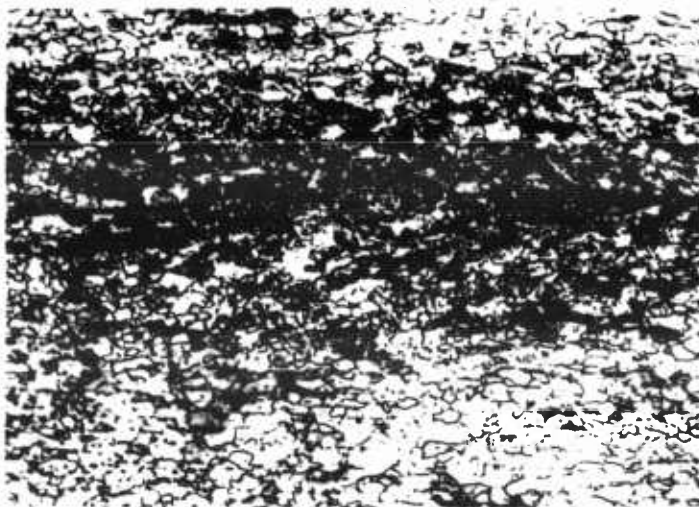
(a) 1020 Steel (0.020-in. thicknesses)
Etchant: 2% Nital
Magnification: 200X
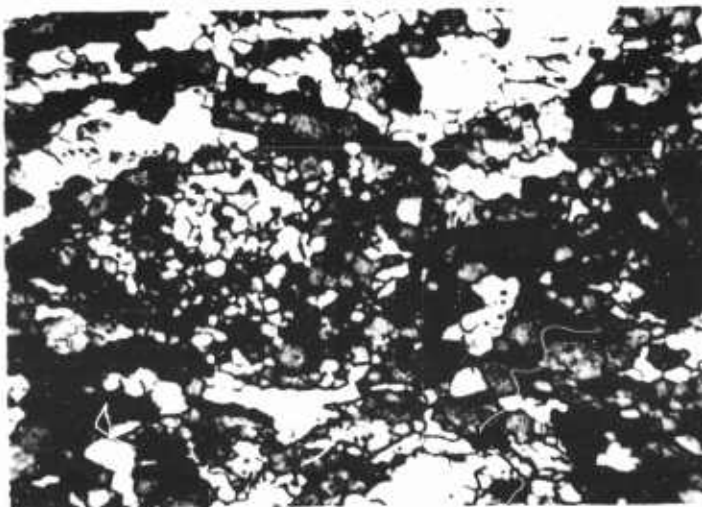
(b) 1020 Steel (0.020-in. thicknesses)
Etchant: 2% Nital
Magnification: 500X

Figure 5. PHOTOMICROGRAPHS OF INTERPENETRATION OF MATING SURFACES
OF 1020 STEEL--SHOWING LOCALIZED RECRYSTALLIZATION
ALONG THE INTERFACE

10

In Figure 6, the weld was made without prior surface preparation between sheets of Inconel X after solution treating and aging. In the aged condition the precipitate appears throughout the grains and preferentially in the grain boundaries. In the neighborhood of the interface, the oxide scale is dispersed and the grain boundaries appear to stop short of the interface.

The precipitate which delineates the boundaries has dissolved in this region. Since solution temperatures for this alloy are in the vicinity of 2100°F, quite high local temperatures apparently were reached in this area. In all cases encountered to date, "etching resistance," not uncommon in an ultrasonic weld, can be explained on the basis of solution of the secondary phase.

Among the microstructural changes attributed to heating is a unique structure developed, apparently, by the vibratory stress acting on the plastic material. The microstructural character of the material is such as to present a block-like appearance. Close examination reveals that the grain boundaries are modified into a zigzag pattern. It appears that the modification or shift of the boundaries into zigzag segments promotes this "block" structure.* The fully developed block structure is shown in Figure 7.

In general, grain and interphase boundaries exhibit smooth curvatures unless there is an orientation dependence; in which case the boundaries would become straight with a direction corresponding to a minimum energy orientation or they may readjust themselves into zigzag straight line segments with each straight segment in a low energy orientation. Only three such cases are known to occur: the coherency boundaries of Widmanstätten structures, the boundaries of twin-related crystals in the face-centered cubic system, and polygonized boundaries.** The chief effect of stress applied at high temperatures is to accelerate polygonization. The motion of dislocation boundaries can either be stress-induced or diffusion-controlled (climb).

Sections of welds in Ti-8 Mn alloy, and 302 stainless steel were examined to determine whether the "block" structure was orientation dependent—i.e., whether the structure was dependent on the vibratory motion of the welding tip and/or the rolling direction of the sheet.

---

* A somewhat similar structure has been observed by Kear and Pratt (Acta Metallurgica, Vol. 6, July 1958) on upquenching a sodium chloride single crystal. These investigators attribute the structure to plastic deformation which produces "wavy slip" bands as they call them. This type of structure is characteristic of deformation above 300°C.

** Another example of a similar structure has been reported by Rogers and Atkins (J. of Met. Trans., p. 620, May 1956). They obtained a striated pattern in quenching a Zr-12% Cb alloy from 1250°C and attributed the structure to rapid cooling through the transformation region.

11

Figure 6. PHOTOMICROGRAPH OF MATING SURFACES OF 0.012-INCH
THICK SHEETS OF INCONEL X AFTER ULTRASONIC WELDING
WITHOUT PRIOR SURFACE PREPARATION—SHOWING OXIDE
DISPERSION IN THE REGION OF THE INTERFACE

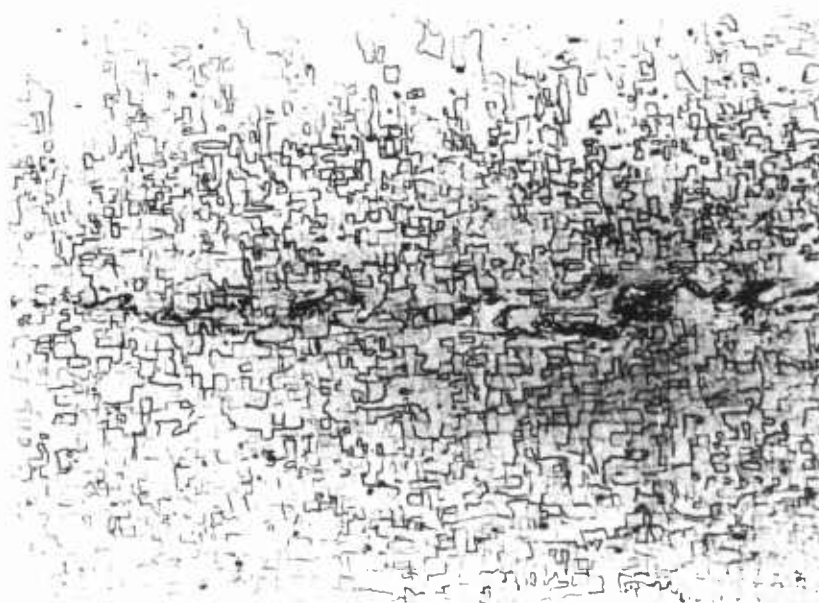Etchant: Oxalic Acid
Magnification: 150X

Figure 7. PHOTOMICROGRAPH OF MATING SURFACES OF TWO THICKNESSES
(0.016 and 0.022 in.) OF TITANIUM-8 MANGANESE ALLOY—
SHOWING MODIFICATION OF THE GRAIN BOUNDARIES DUE TO
HEATING DURING ULTRASONIC WELDING

Etchant: HF + HNO$_3$
Magnification: 150X

It was observed that the rolling direction had no effect on the development of the structure; however, the pattern was different in sections taken longitudinally and transversely to the direction of vibratory motion. In the longitudinal sections the boundaries tend to be arranged in directions parallel and normal to the interface; the orientation of the boundaries is more random in sections normal to the vibratory direction. Figures 8 and 9 show this orientation effect.

The "block" structure has been observed in the fcc alloys K-Monel, 302 stainless steel, 2024 aluminum, Inconel X, L-605, Imco 792, and the bcc phase of the Ti-8 Mn alloy.*

The question of diffusion reactions during welding is difficult to resolve on the basis of known static diffusion coefficients. The short welding times tend to dissuade one from the view that diffusion on an observable scale could take place. However, the influence of ultrasonics on diffusion phenomena must be considered, and, although the literature is relatively barren in this regard, a possible accelerating effect cannot be ignored. Several clear examples of diffusion occurring during welding have been observed.

The observations of diffusion between copper and zinc presented in Reference (7) have been supplemented by the indication of diffusion which occurs in another weld system. A weld made between a 0.030-inch thick sheet of type O-2 tool steel** and 0.030-inch Armco iron is shown in Figure 10. The welding parameters were 4200 watts, 600 pounds clamping force, and 1.5 seconds exposure time. Compared to the welds between the aluminum copper alloy, this system would be expected to possess several advantages as a diffusion couple because of the existing concentration gradient, low thermal conductivity which would be expected to result in a higher temperature rise, and, in the present case, an increase in input power of 50 percent. Whether thermal diffusion in weld couples is necessary to achieve bonding or simply is a result of temperatures generated at the interface is a question which must be answered on the basis of the characteristics of monometal welds. In this respect, evidence to date indicates that the latter viewpoint is most consistent with the experimental observations. No evidence by either metallographic or autoradiographic examination has indicated that material transport by thermal diffusion is necessary for bonding in monometal weld couples. On the contrary, diffusion (neglecting recrystallization and growth phenomena or phase transformations) has been observed only in the two cases cited above in which power levels were very high and the weld members were dissimilar materials.

---

* Polonis and Parr (J. of Met. Trans., p. 514, May 1956) have observed a block-type pattern in retained β phase of Ti-Mn alloys. They compare the structure to a similar one obtained by Barrett in Cu-Si alloys (Imperfections in Nearly Perfect Crystals (1952) p. 97, John Wiley and Sons, Inc., New York) which was interpreted as clusters of faults separated by relatively perfect crystal layers. Internal strain from quenching was proposed as an explanation of the origin of the structure.

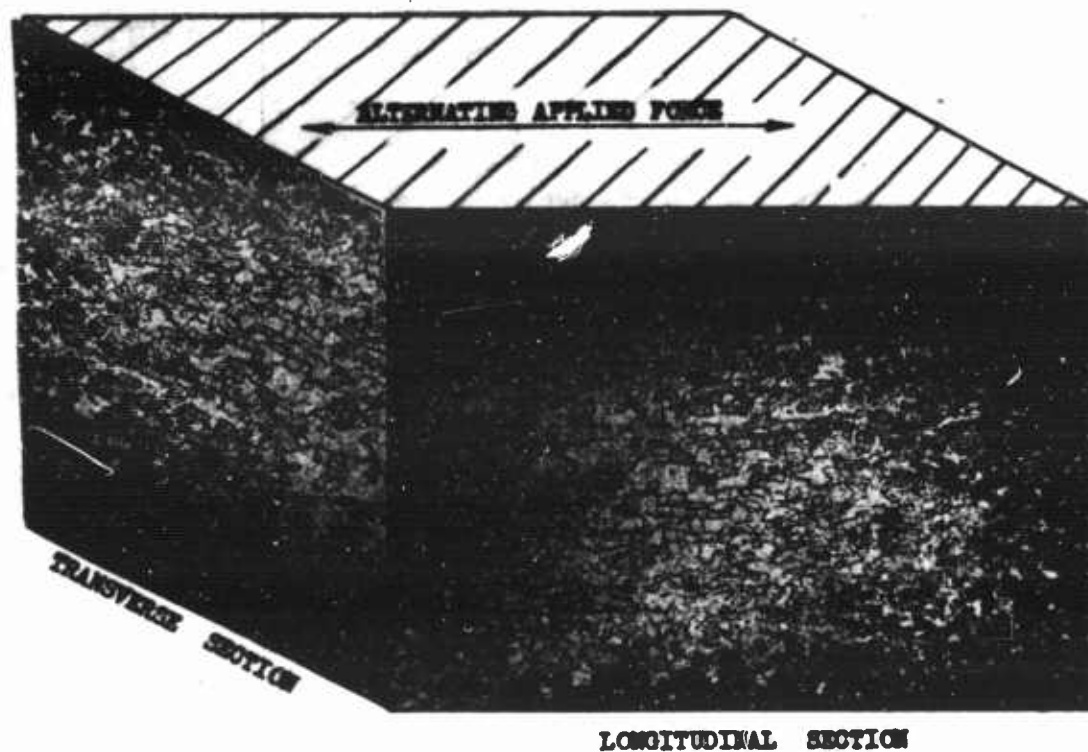** Simmonds Oil Hardening Die Steel.

Figure 8. PHOTOMICROGRAPHS OF 0.020-INCH THICKNESSES OF TITANIUM-
8 MANGANESE ALLOY SECTIONS TAKEN TRANSVERSELY AND
LONGITUDINALLY TO THE VIBRATORY MOTION OCCURRING DURING
ULTRASONIC WELDING--SHOWING BLOCK-LIKE ORIENTATION
EFFECT

Etchant: HF + HNO$_3$
Magnification: 100X

15

Figure 9. PHOTOMICROGRAPHS OF 0.025-INCH THICKNESSES OF 302 STAINLESS STEEL TAKEN TRANSVERSELY AND LONGITUDINALLY TO THE VIBRATORY MOTION OCCURRING DURING ULTRASONIC WELDING--SHOWING BLOCK-LIKE ORIENTATION EFFECT

Etchant: Oxalic Acid
Magnification: 100X
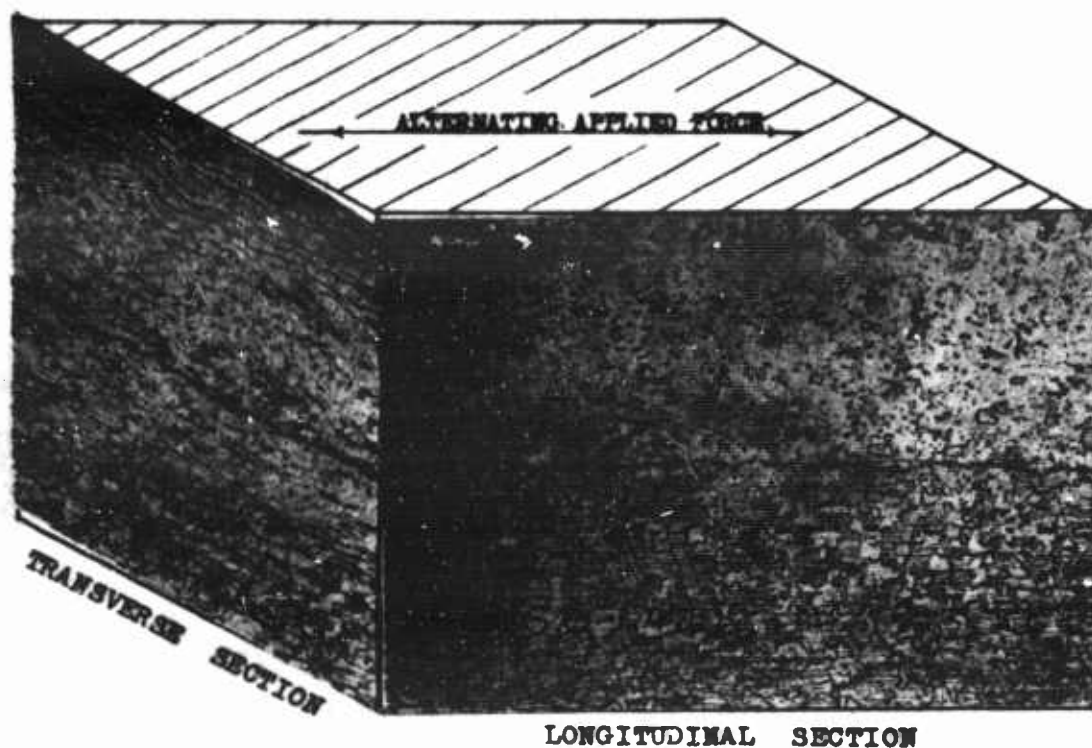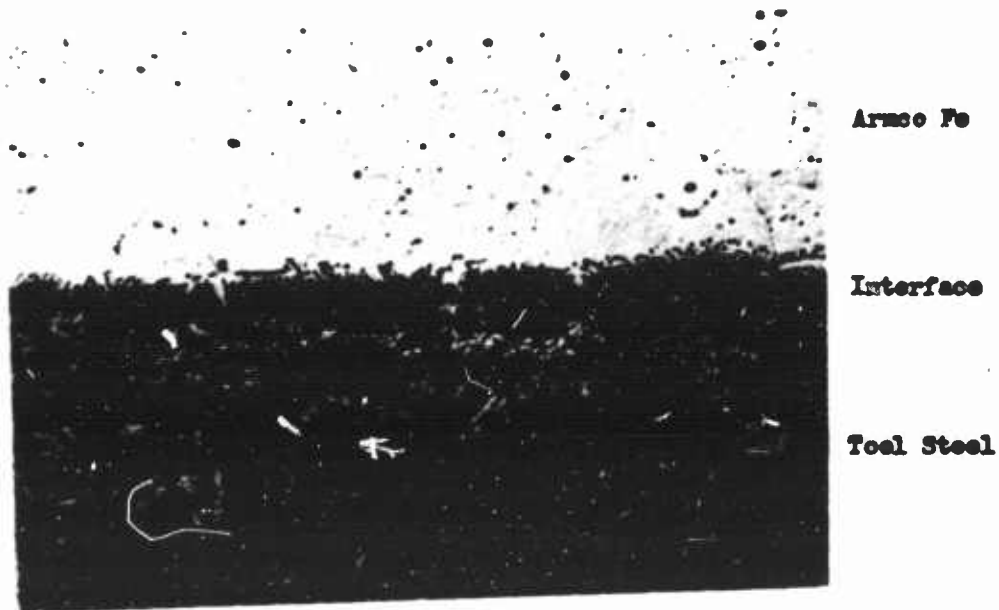
Figure 10. PHOTOMICROGRAPH OF ULTRASONIC WELD BETWEEN 0.030 INCH
AISI TYPE O-2 TOOL STEEL (.90% C) AND 0.030 INCH ARMCO
IRON--ILLUSTRATING THE TRANS-INTERFACIAL DIFFUSION OF
CARBON INTO THE IRON

Etchant: Picral
Magnification: 1000X

17

A more fundamental question involves the role of the surface films or scale in the bonding mechanism, since nascent metal contact is presumed necessary for bonding to occur. The discontinuities in the barrier films are brought about by the relative displacements imposed by the vibratory action of the active sonotrode. The degree of film disruption depends in part on controllable factors such as the welding parameters and on the inherent properties of the film and substrate material. The influence of film hardness on the ease of pressure welding has been discussed by Tylecote (8), the influence of oxide hardness on sliding friction has been reviewed by Whitehead (9) and Bowden (10).

Knowledge of the significance of oxide thickness on power requirements for welding is desirable; therefore, an experiment is presently in preparation in which the influence of various thickness of anodised coatings on aluminum will be determined. The breakup and dispersion of the oxide film will be followed by impregnation of the film with a radioactive tracer. Arrangements are being made for the preparation of the specimens with controlled oxide thickness and the license for handling the radio-active isotope has been applied for.

Thus we see that bonding is usually accompanied by local working and heating effects, interruption and displacement of oxide or other barrier films, and, in some cases, extrusion of plastic metal from the bond zone (not illustrated).

The temperature effect is important. When bond temperatures are attained which are below the recrystallisation temperature, cold work effects such as mechanical twinning, deformation bonds, and grain distortion occur. Occasionally, temperatures which seemingly do not far exceed the recrystallisation temperature are achieved; in this case, a recrystallised zone along the interface has been observed. It is presently believed that higher temperatures are necessary to permit the edge extrusion phenomenon. This view is consistent with the observation that extrusion has been noted in these materials whose weld temperature can be inferred on the basis of phase transformation.

In conclusion, the following effects have been observed in ultrasonic welds:

1. Interfacial phenomena

   (a) surface film dispersion
   (b) interpenetration

2. Working effects

   (a) plastic flow and grain distortion
   (b) edge extrusion

18

3. **Heat effects**

    (a) recrystallization
    (b) precipitation
    (c) phase transformation
    (d) diffusion

4. Others not specifically identified.

C. MATERIAL PROPERTIES AND WELDABILITY

After the SWR power measurement technique was developed in Phase I of this program, it was utilized in preliminary studies to determine the net acoustical energy required to generate a unit area of weld in aluminum, copper, and 302 stainless steel, in each of several thicknesses.

The procedure is to:

(a) Establish characteristic curves of electrical power required to produce good welds (as defined by nugget pull-out in a peel test) as a function of clamping force. From such a curve for each gage of each material, the minimum electrical power that reproducibly produces a good weld is selected. Summary data of minimum electrical power required to simply produce a weld (without regard to its area) is routinely presented as a function of gage as will be evident later.

(b) Apply the SWR technique at the minimum electrical power value, and ascertain reproducibly the net acoustical energy required to generate a weld without regard to its area (11).

(c) Ascertain the actual area of the weld envelope from specimens obtained in (b) above.

(d) Compute the net acoustical energy required to produce a weld of unit area.

It must be noted that constant weld time and tip radii combinations are maintained. Moreover, energy passing through and beyond the weld zone is presently included in all such data presented. This loss factor is being carefully considered (12).

The required minimum electrical power determinations to make a weld as from (a) above are summarized as in Figure 11, which includes the preliminary data (13) obtained in Phase I. New data on several materials available at the outset of Phase II are also presented in Figure 11. Thus, a crude "order-of-weldability," based on electrical power to the transducer, is becoming evident.

19

Legend:

- ⊙ – 1100-H18-19
- + – 1100-0
- A – Au-.6% Sb
- B – Au-.6% Ga
- x – CP Cu
- C – COIN SILVER
- P – PERMALLOY
- E – Be-Cu
- ▲ – 302 SS
- Z – ZIRCONIUM

Y-axis: MINIMUM ELECTRIC POWER – WATTS (10,000 / 1000 / 100 / 10 / 1.0 / 0.1)

X-axis: SHEET THICKNESS – INCH (0.0001 / 0.001 / 0.01 / 0.10)

FIGURE 11. MINIMUM AVERAGE ELECTRIC POWER TO WELD THIN GAUGES OF TEN MATERIALS
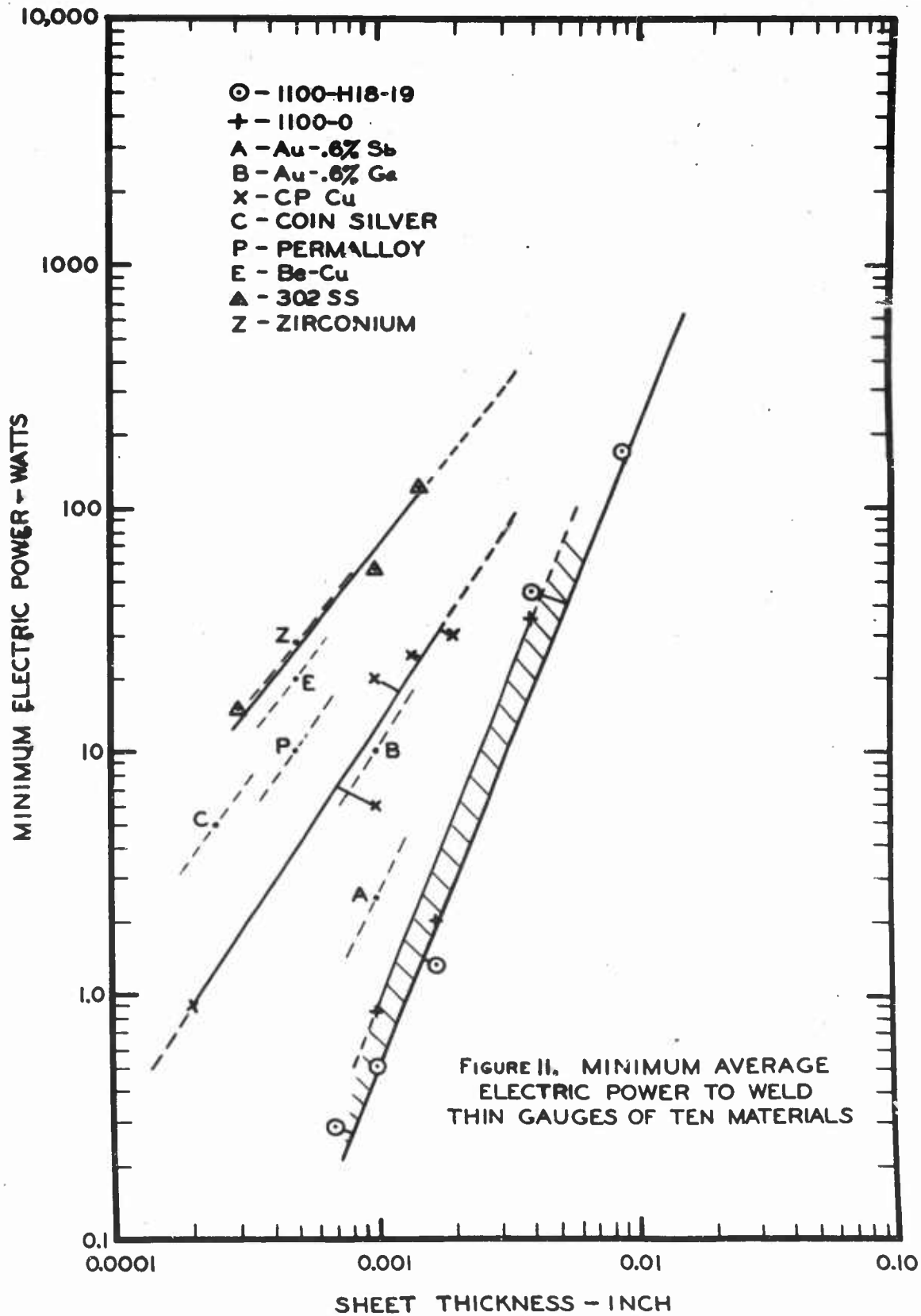
Table 1 lists in order of electrical power required to make a weld, the materials so far studied, together with Vickers microhardness data, for room temperature conditions.

Table 1

MICROHARDNESS DATA

(Listed in the order of electrical power required to make a weld)

	Microhardness	
	Published*	Measured
1100-H18-19	45-50	--
1100-0	20-25	--
Au-.6% Sb (Hard)	--	112
Au-.6% Ga	--	102.5
C.P. Cu (1/2 H)	75-85	79.5
Coin Silver (.002)	109-150	138
Permalloy	--	412
Be-Cu	220-230	250
302-SS (3/4 H)	--	360
Zirconium	220-240	--

* Converted to equivalent Vickers' microhardness data.

The "order-of-weldability" presented in the list of materials of Table 1 will be altered when:

(a) the effect of weld area is introduced,
(b) net acoustical energy is used,

and the order is set by net acoustical energy per unit weld area instead of by electrical power required to make a weld. For example, larger welds are effected in soft 1100-0 than in the harder 1100-H18. Thus, when the data is reduced to power per unit area, this discrepancy within the aluminum group will disappear. Moreover, there will be some additional correction when the figures are corrected for energy passing through and beyond the weld zone into the reflector anvil system.

It is not here implied or indicated that an ultimate "order-of-weldability" will correlate with hardness or with any single property whatever, for that matter. The problem is complex; properties at temperature such as elastic modulus, shear yield, thermal diffusivity, and others are being considered.

Reduction of electrical power data, such as above, to net acoustical energy per unit weld area is proceeding, and summary data on the latter for all the above and other materials will appear in forthcoming reports.

III. PLANS FOR NEXT PERIOD

During the next period, effort will be expended to:

1. Complete photoelastic analysis for the normal loading condition without transverse load, i.e., normal stress and shearing stress. For the normal plus transverse load prior to slip, compute normal and shearing stress at interface.

2. Develop net acoustical energy data for materials covered in Subsection IIC, of this report.

3. Develop additional electrical power data for other materials (2 thicknesses of tantalum, 0.005 and 0.010 inch; and 0.010-inch thickness of Molybdenum).

4. Initiate the acquisition of weld zone temperature data during determination of minimum electrical power and net acoustical energy.

5. Initiate experiments to determine the fraction of power lost via the anvil system for several materials.

It is expected that Phase II of the program, Fundamentals of Ultrasonic Welding, as outlined in the current contract will be finished on schedule and within the funds allocated.

22

LIST OF REFERENCES

1. Aeroprojects Incorporated, "Fundamentals of Ultrasonic Welding," Bimonthly Report No. 2, February 1958 (Navy, BuAer Contract NOas 58-108-c), Figure 1.

2. Ibid., pp. 1-6.

3. Frocht, M. M., Photoelasticity, New York: John Wiley & Sons Inc., 1946, Vol. I, pp. 148-149, 254.

4. Timoshenko, S., and Goodier, J. N., Theory of Elasticity, New York: McGraw-Hill Book Co., 1951, p. 99.

5. Lee, G. H., An Introduction to Experimental Stress Analysis, New York: John Wiley & Sons Inc., 1956, p. 192.

6. Ibid., p. 209.

7. Aeroprojects Incorporated, "Fundamentals of Ultrasonic Welding", Bimonthly Report No. 2, February 1958 (Navy, BuAer Contract NOas 58-108-c), Figure 9.

8. Tylecote, M. A., "Investigations on Pressurized Welding", British Welding Journal, March 1954.

9. Whitehead, J. R., Proc. Roy. Soc., 1950, Vol. 201-A, pp. 109-124.

10. Bowden, F. P., "Properties of Metallic Surfaces", Inst. of Metals Monograph, 1953, pp. 197-212.

11. Aeroprojects Incorporated, "Fundamentals of Ultrasonic Welding", Bimonthly Report No. 4, June 1958 (Navy, BuAer Contract NOas 58-108-c), pp. 1-6 and 9-14.

12. Idem, Bimonthly Report No. 1, December 1957, p. 10; Bimonthly Report No. 2, January 1958, p. 9; Bimonthly Report No. 3, April 1958, p. 10; and Bimonthly Report No. 5, August 1958, p. 3.

13. Idem, Bimonthly Report No. 6, October 1958, Figure 4.

UNCLASSIFIED

AD

220 210

UNCLASSIFIED